

## The ATIC experiment: Performance of the scintillator hodoscopes and the BGO calorimeter.

J. Isbert (for the ATIC collaboratio)

Louisiana State University, Baton Rouge, LA 70803 USA

### 1 Abstract

The Advanced Thin Ionization Calorimeter (ATIC) Balloon Experiment had its first flight from McMurdo, Antarctica 28/12/2000 to 13/01/2001, local time, recording over 360 hours of data. The design goal of ATIC was to measure the Cosmic Ray composition and energy spectra from ~50 GeV to near 100 TeV utilizing a Si-matrix detector, a scintillator hodoscope, carbon targets and a calorimeter consisting of a stack of BGO scintillator crystals. The design, the operations and in-flight performance of the scintillator hodoscope and the BGO calorimeter are described.

### 2 The ATIC design

ATIC is designed primarily to measure cosmic ray spectra for elements from hydrogen to nickel. The measurement technique used is ionization calorimetry. Cosmic rays interact with a low Z target, produce secondary pions which then start a shower in the calorimeter.

In order to determine these spectra the following quantities need to be measured:

- 1) The charge of the individual cosmic ray particle,
- 2) Its energy and
- 3) The abundance of each species.

The ATIC balloon instrument is composed of two major subsystems: the target module and the calorimeter.

The target module has 4 functions:

- 1) Force the incoming cosmic ray to interact
- 2) Determine the charge of the incoming cosmic ray,

- 3) Provide a trigger for the instrument
- 4) Provide tracking in combination with the calorimeter.

The calorimeter has 2 functions:

- 1) Determine the energy of the cosmic ray,
- 2) Provide tracking in combination with the target module.

### 2.1 The target module

The target module consists of (from top to bottom): a silicon matrix array, a plastic scintillator XY plane, 10cm of carbon target, a 2<sup>nd</sup> scintillator XY plane, 20cm of carbon target and a 3<sup>rd</sup> scintillator XY plane. The Silicon matrix is the primary charge detector, supplemented by the topmost scintillator plane.

A potential problem for charge determination in the presence of calorimeters are particles back scattered from the shower into the detectors above once the energy of the cosmic ray exceeds a few TeV. Simulations of high energy protons in the ATIC experiment indicate that, indeed, as the proton energy increases the number of "back-splash" particles per unit area increases in all three scintillator planes as well as the silicon matrix detector, potentially adding to the charge signal and degrading the ability to distinguish between protons and Helium. To combat this effect both charge detectors are segmented, thereby decreasing the probability of back scattered particles passing through the same detector element as the cosmic ray.

The Silicon matrix consists of 4480 individually read out pixels (Adams et al, 1999). The scintillator detectors consist of individual strips. **Fig. 1** shows the bottom half of one scintillator XY plane. It consists of individual strips of plastic scintillator read out by photomultiplier tubes at each end. The front end electronics is mounted directly behind the photomultipliers and consists of preamplifiers, ADCs and discriminator outputs for the trigger logic. One plane consists of two such halves rotated 90 degrees to each other.



**Fig. 1:** Top view of one half of a hodoscope plane

## 2.2 The Calorimeter

The calorimeter module consists of a "package" of 320 BGO crystals, each 2.5 cm by 2.5 cm by 25 cm in size and placed into 8 trays of 40 crystals each, covering an active area of 51 x 51 cm<sup>2</sup>. Alternating layers are rotated 90 degrees relative to each other to form 4 X and 4 Y layers. **Fig.2** shows a bottom view of the assembled ATIC instrument showing the 4 X and 4 Y palnes of the calorimeter at the bottom as well as the instrument electronics distributed around the detectors.

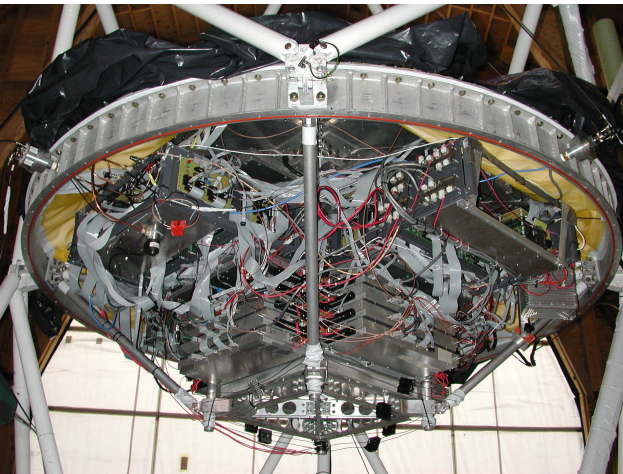


**Fig. 2:** Side view of the assembled ATIC experiment.

Each BGO crystal is wrapped in teflon tape and covered with aluminum coated mylar foil for light tightness. Each crystal is viewed by a photomultiplier tube (PMT), Hamamatsu R5611-01 placed into a front end electronics box which is mounted directly to each tray. A light attenuator is placed on the front face of each photomultiplier to keep the readout linear over the entire signal range. A light emitting diode (LED) is mounted onto the side of the PMT for calibration and liveliness tests.

To measure particle energies up to 100 TeV the readout device has to cover energy deposits from about 5 MeV to over 10 TeV in each individual crystal. This high dynamic range of the signals in a single crystal of  $2 \times 10^6$  forces the readout of the photomultiplier tube (PMT) to be split into three gain ranges. This is accomplished by utilizing three dynode pickoffs and feed them into different preamp channels.

The absolute energy calibration of the calorimeter is done by utilizing cosmic ray muons. First the energy deposit per

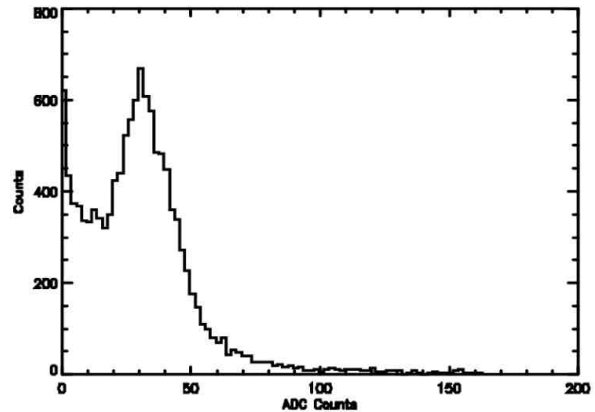


**Fig. 3:** Pulseheight distribution for cosmic ray muons in low energy range

ADC count is determined for the low energy range of every BGO crystal. Figure 3 shows an example of a muon spectrum for the low energy range.

Then the higher energy ranges (=lower gain) are calibrated using the overlap between ranges. **Fig.4** shows the

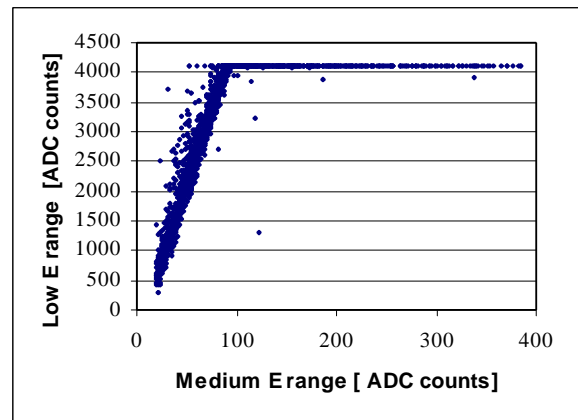


**Fig. 4:** Pulseheight low E range vs medium E range

pulseheight of the low energy range versus the medium energy range. The slope in the linear region determines the ratio of low E range to medium E range. The ratio of the high E range to the medium range is determined using the overlap region of these ranges. **Fig. 5** shows the pulseheight of the medium E range vs the high E range.

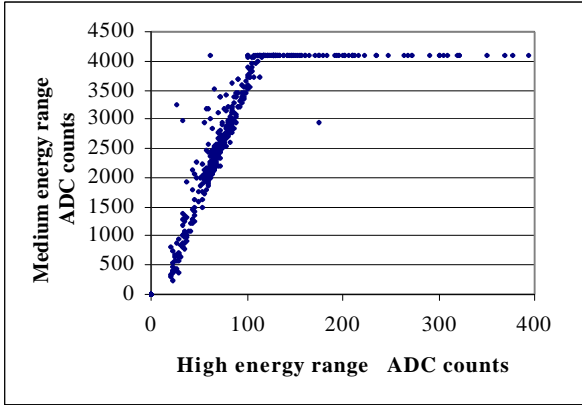


**Fig. 5:** Pulseheight medium E range vs high E range

Utilizing this bootstrapping calibration mechanism, it is possible to determine the deposited energy of particle showers in the fully active BGO calorimeter very accurately.

Both modules provide tracking of the incident cosmic ray. The plastic scintillator strips provide 3 X coordinates and 3 Y coordinates which are simply derived from the hit pattern in each plane. The BGO calorimeter planes provide 4 X and 4 Y coordinates. Each coordinate is derived via a centroid scheme from the crystal signals in each plane.

**3) The ATIC Trigger**

The ATIC experiment trigger needs to fulfill two requirements:

- 1) It must trigger on potential events which pass through the active aperture of ATIC, and
- 2) It has to set an energy threshold

Requirement 1 is fulfilled by deriving a trigger from the scintillator hodoscope.

Requirement 2 is fulfilled by utilizing discriminators on the BGO crystals and form an energy dependant trigger signal.

These two triggers are formed separately due to their different timing characteristics. The plastic scintillator hodoscope form a pre-trigger derived from the topmost scintillator plane (S1) in coincidence with the scintillator plane below the carbon target (S3). This pre-trigger (PT) also locks the preamp outputs for potential readout.

The energy dependant trigger, the master trigger (MT) is formed from the discriminator outputs of the BGO crystal readout preamplifiers.

**Fig.6** shows the data collection rate over the flight of ATIC. In the beginning of the flight while high-speed line of site communication was available several trigger scheme and threshold combinations were tried to determine the best flight trigger. Shortly before the line of site communication went out of range the flight trigger and threshold combination was set. The energy threshold was changed twice during operation to adjust the fill rate of the hard disk in order to collect data over the anticipated duration of the flight. Shortly before termination of the flight a different trigger and threshold scheme was set to study their effectiveness.

**4) Summary**

The ATIC instrument had a very successful long duration balloon flight from Mcmurdo, Antarctica. All detectors and their support systems worked well over the entire flight.

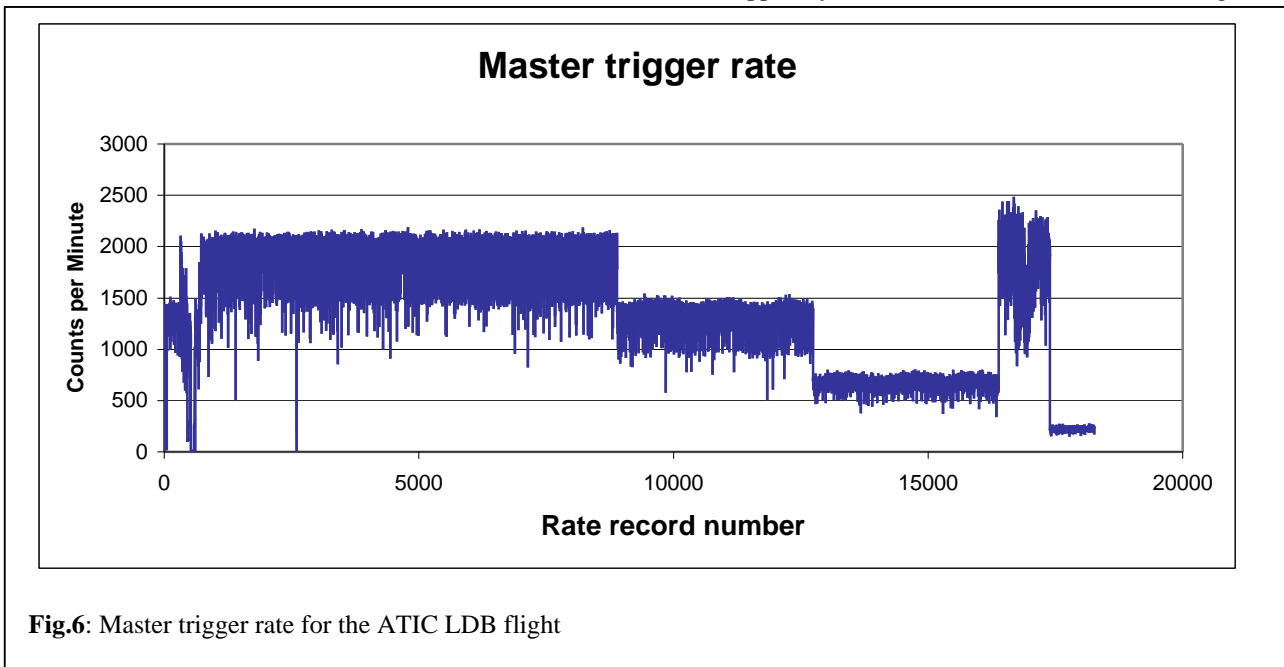


**Fig.6:** Master trigger rate for the ATIC LDB flight

**References:**

- Adams, J. H. et al., the ATIC Collaboration, Proc. 26<sup>th</sup> Int. Cosmic Ray Conf. (Salt Lake City), **5**, 69 and 76, 1999.
- Ganel, O. et al., The ATIC Collaboration, Proc. 26<sup>th</sup> Int. Cosmic Ray Conf. (Salt Lake City), **5**, 453, 1999.
- Ganel, O. et al., The ATIC Collaboration, Adv. In Space Research, in press, 2001.
- Guizk, T. G. et al., the ATIC Collaboration, SPIE International Symposium on Optical Science, Engineering, and Instrumentation, Denver, CO, **2806**, 122, 1996.
- Guizk, T. G. et al., the ATIC Collaboration, Proc. 26<sup>th</sup> Int. Cosmic Ray Conf. (Salt Lake City), **5**, 6, 1999.
- Seo, E. S. et al., the ATIC Collaboration, SPIE International Symposium on Optical Science, Engineering, and Instrumentation, Denver, CO, **2806**, 134, 1996.
- Seo, E. S. et al., the ATIC Collaboration, Advances in Space Research, **19**, No. 5, 711, 1997.